In K. M. Hanson, Medical Imaging 1999 – Image Processing, San Diego, USA

Nonrigid matching of tomographic images based on a biomechanical model of the human head

A. Hagemann[1], K. Rohr[1], H. S. Stiehl[1], U. Spetzger[2], J. M. Gilsbach[2]

[1]Universität Hamburg, FB Informatik, AB Kognitive Systeme,
Vogt-Kölln-Straße 30, D-22527 Hamburg, Germany
Tel.: +49 (40) 42883 2577 Fax: +49 (40) 42883 2572
E-Mail: hagemann@informatik.uni-hamburg.de

[2]Neurochirurgische Klinik, Universitätsklinik der
Rheinisch-Westfälischen Technischen Hochschule (RWTH),
Pauwelstraße 30, D-52057 Aachen, Germany

ABSTRACT

The accuracy of image-guided neurosurgery generally suffers from brain deformations due to intraoperative changes, e.g., brain shift or tumor resection. In order to improve the accuracy, we developed a biomechanical model of the human head which can be employed for the correction of preoperative images. By now, the model comprises two different materials. The correction of the preoperative image is driven by a set of given landmark correspondences. Our approach has been tested using synthetic images and yields physically plausible results. Additionally, we carried out registration experiments with a preoperative MR image and a corresponding postoperative image simulating an intraoperative image. We found, that our approach yields good prediction results, even in the case when correspondences are given in a small area of the image only.

Keywords: elasticity theory, biomechanical model, inhomogeneous materials, finite element method, intraoperative image correction

1. INTRODUCTION

The accuracy of image-guided neurosurgery generally suffers from brain deformations due to intraoperative changes like brain shift or tumor resection, which generally result in large changes of the brain anatomy, see e.g. Hill et al.[1] To improve upon navigation accuracy, we developed a biomechanical model of the human head which allows to predict intraoperative brain deformations and thus to correct the preoperative image w.r.t. surgery-induced effects.

Recent work in the field of intraoperative image correction comprises different models of the human head, which distinguish between anatomical structures with variable material properties. Some of these head models are based on physical motivations only, like mass-spring systems[2] or a combination of different energy terms.[3] However, these types of models incorporate no real physical material parameters and hence are only weakly related to the physical behaviour of biological soft tissue. In contrast to these physically motivated models, there are other approaches, which are based on a direct physical description of the material behaviour.

One approach is the model of Davatzikos,[4] where linear elasticity theory is used as physical basis. Additional terms for modelling of material inhomogeneities were introduced into the equilibrium description of the underlying linear elastic body. The resulting equations were then solved by successive overrelaxation. Despite the general difficulty to determine forces from images, Davatzikos applied image derived forces to drive the deformation of the linear elastic body. As material parameter values, the author used heuristic values. Another recent approach is developed by Kyriacou and Davatzikos[5] which used the Mooney-Rivlin strain energy function[6,7] for the simulation of incompressible materials. However, the authors set the second Mooney-Rivlin parameter to zero which is in contrast to the value determined, and compared against reported measurements[8] by Mendis et al.[7] The resulting equations are solved by the finite element method. Instead of explicitly modelling different anatomical structures, the authors introduced appropriate boundary conditions, e.g., the dura mater is integrated as a non moving part (known as *homogeneous Dirichlet boundary condition*) and there is no movement between the dura mater and the brain at the contact surface allowed (so called *no-slip boundary condition*). The model of Lester et al.[9] is based on an inhomogeneous viscous fluid model, i.e. modified Navier-Stokes equations, with locally varying viscosity parameters

for the simulation of different anatomical structures. Also here, forces were used to drive the deformation and the resulting equations are solved by successive overrelaxation. An apparent problem with this model is the assumption that all anatomical structures behave like a viscous fluid which is generally not the case. Škrinjar et al.[10] used a set of mass nodes connected by Kelvin models to simulate the behaviour of brain tissue. A Kelvin model is a simplified mechanical model[11,12] for viscosity and consists of a parallel connection of a linear spring and a dashpot. The deformation is driven by applied forces and different anatomical structures are modelled by appropriate boundary conditions only.

Our approach is based on the well-established physical theory of continuum mechanics to handle inhomogeneous materials. We apply the finite element method for discretization, resulting in a large linear matrix system. Instead of using forces, which are generally difficult to determine from images, we use a set of given correspondences to drive the deformation of the preoperative image. According to the underlying anatomical structure, different materials were incorporated by physically connecting homogeneous subregions by appropriate boundary conditions. The necessary material parameter values were determined through a comprehensive literature study. Prior to our registration experiments with clinical 2D pre- and postoperative MR images, we carried out experiments with synthetic 2D images in order to assess the physical plausibility of the deformations predicted by our model.

2. APPROACH

Our biomechanical model is based on the *equations of motion*, which describe the deformation of a body Ω under externally applied forces,

$$\begin{cases} -\operatorname{div}\boldsymbol{\sigma} = \mathbf{f} & \text{in}\,\Omega, \\ \boldsymbol{\sigma}\,\mathbf{n} = \mathbf{g} & \text{on}\,\Gamma, \end{cases} \tag{1}$$

where $\boldsymbol{\sigma}$ denotes the *Eulerian stress tensor*, $\mathbf{f}$ the applied body forces, $\mathbf{n}$ the unit vector normal to the surface Γ, and $\mathbf{g}$ the forces acting on Γ. To incorporate material properties of Ω, the appropriate *constitutive equation*, which describes the stress/strain relationship of the body, has to be substituted into the equations of motion. Assuming - as a first approximation - linear elastic material properties, we apply Hooke's law

$$\boldsymbol{\sigma} = \lambda(\operatorname{tr}\mathbf{e}(\mathbf{u}))\mathbf{I} + 2\mu\mathbf{e}(\mathbf{u}), \tag{2}$$

to the equations of motion thus yielding the system

$$\begin{cases} -\operatorname{div}[\lambda(\operatorname{tr}\mathbf{e}(\mathbf{u}))\mathbf{I} + 2\mu\mathbf{e}(\mathbf{u})] = \mathbf{f} & \text{in}\,\Omega \\ (\lambda(\operatorname{tr}\mathbf{e}(\mathbf{u}))\mathbf{I} + 2\mu\mathbf{e}(\mathbf{u}))\mathbf{n} = \mathbf{g} & \text{on}\,\Gamma. \end{cases} \tag{3}$$

Here, λ and μ denote the common *Lamé constants*, $\mathbf{u}$ the unknown displacement vector field, $\mathbf{e}(\cdot)$ *Cauchy's infinitesimal strain tensor*, $\mathbf{I}$ the identity matrix, and $(\operatorname{tr}\cdot)$ the trace operator.

In order to solve the equations of motion for the unknown function $\mathbf{u}$ within a sufficient smooth function space, we use the *method of weighted residuals*.[13,14] With this method, we demand that the projection, i.e. the inner product $\langle\cdot,\cdot\rangle$, of the residuum onto arbitrary weighting functions $\mathbf{w}$ of the function space vanishes over the body Ω:

$$\int_\Omega \langle -\operatorname{div}\left[\lambda(\operatorname{tr}\mathbf{e}(\mathbf{u}))\mathbf{I} + 2\mu\mathbf{e}(\mathbf{u})\right] - \mathbf{f}, \mathbf{w}\rangle \, d\Omega = 0. \tag{4}$$

After some calculus, this can be transformed into

$$\int_\Omega \lambda(\operatorname{tr}\mathbf{e}(\mathbf{u}))(\operatorname{tr}\mathbf{e}(\mathbf{w})) + 2\mu\langle\mathbf{e}(\mathbf{u}), \mathbf{e}(\mathbf{w})\rangle \, d\Omega = \int_\Omega \langle\mathbf{f}, \mathbf{w}\rangle \, d\Omega + \int_\Gamma \langle\mathbf{g}, \mathbf{w}\rangle \, d\Gamma. \tag{5}$$

By application of the *Galerkin method*, i.e. using only a finite dimensional subspace spanned by a finite number of basis functions $\boldsymbol{\phi}_i$, we can approximate the function $\mathbf{u}$ by a finite sum of basis functions $\boldsymbol{\phi}_i$ multiplied with unknown coefficients u_i,

$$\mathbf{u} = \sum_i u_i \boldsymbol{\phi}_i. \tag{6}$$

Substitution of this approximation into (5) and choosing a weighting function $\mathbf{w}$ represented by $\sum_j \boldsymbol{\phi}_j$, leads to the expression

$$\sum_i u_i \int_\Omega \lambda(\operatorname{tr} \mathbf{e}(\boldsymbol{\phi}_i))(\operatorname{tr} \mathbf{e}(\boldsymbol{\phi}_j)) + 2\mu\langle \mathbf{e}(\boldsymbol{\phi}_i), \mathbf{e}(\boldsymbol{\phi}_j)\rangle \, d\Omega = \int_\Omega \langle \mathbf{f}, \boldsymbol{\phi}_j\rangle \, d\Omega + \int_\Gamma \langle \mathbf{g}, \boldsymbol{\phi}_j\rangle \, d\Gamma, \tag{7}$$

which can be written in compact matrix notation as

$$\mathbf{A}\mathbf{u} = \mathbf{f} + \mathbf{g}, \tag{8}$$

where the matrix $\mathbf{A}$ is commonly known as *stiffness matrix*.

So far, the derived linear equation system (8) contains the description of a *homogeneous*, linear elastic body only. By dividing an inhomogeneous body Ω into a set of homogeneous subregions Ω_i according to the underlying anatomical structure, we are able to simulate inhomogeneous material behaviour with our model. Therefore, all subregions Ω_i are physically linked by the *compatibility* and *equilibrium* boundary conditions[12,14]: The former condition states, that the displacements $\mathbf{u}^\Gamma$ at the common boundary Γ between two subregions Ω_1 and Ω_2 must be equal, while the latter one states that in the equilibrium, the sum of all stress vectors acting on the boundary Γ must be zero. Introduction of these boundary conditions and assuming homogeneous body forces $\mathbf{f}$ over $\Omega = \Omega_1 \cup \Omega_2$ allows to couple both linear systems, ending up with one overall linear equation system:

$$\underbrace{\begin{pmatrix} \mathbf{A}_{11}^1 & \mathbf{A}_{1\Gamma}^1 & \mathbf{0} \\ \mathbf{A}_{\Gamma 1}^1 & \mathbf{A}_{\Gamma\Gamma}^1 + \mathbf{A}_{\Gamma\Gamma}^2 & \mathbf{A}_{\Gamma 2}^2 \\ \mathbf{0} & \mathbf{A}_{2\Gamma}^2 & \mathbf{A}_{22}^2 \end{pmatrix}}_{\mathbf{A}} \underbrace{\begin{pmatrix} \mathbf{u}^1 \\ \mathbf{u}^\Gamma \\ \mathbf{u}^2 \end{pmatrix}}_{\mathbf{u}} = \underbrace{\begin{pmatrix} \mathbf{f} + \mathbf{g}^1 \\ \mathbf{f} \\ \mathbf{f} + \mathbf{g}^2 \end{pmatrix}}_{\mathbf{b}}. \tag{9}$$

With $\mathbf{A}_{11}^1$ etc., we denoted the submatrices of the corresponding stiffness matrices $\mathbf{A}^1$ and $\mathbf{A}^2$ for the subregions Ω_1 and Ω_2, respectively. An index Γ, as appearing in $\mathbf{A}_{1\Gamma}^1$ etc., indicates those submatrices which comprise finite elements belonging to the common boundary Γ between both subregions. Due to the underlying pixel grid of the images, we used quadrilateral finite elements with four nodes, i.e. bilinear interpolation functions $\boldsymbol{\phi}_i$ to approximate the functions $\mathbf{u}$ and $\mathbf{w}$. After substitution of the given boundary conditions, the linear matrix system (9) can be solved for the unknown displacements $\mathbf{u}$ by using the numerical method of conjugate gradients.

To calculate the deformation of an anatomical structure due to given spatial correspondences between images, these correspondences must be integrated into the linear equation system. To this end, we use the procedure described in Peckar et al.[15]: Given a value for the unknown u_j, this can be incorporated into the linear equation system by a subtraction of the product $u_j\mathbf{A}_j$, where $\mathbf{A}_j$ denotes the j-th column of the stiffness matrix $\mathbf{A}$, from the righthand side vector $\mathbf{b}$, followed by a substitution of the given value into the j-th row of $\mathbf{b}$. Thereafter, the j-th row and column of $\mathbf{A}$ are set to zero and, respectively, the diagonal element A_{jj} to one. By repeating this procedure for a set of correspondences, to be given at the surface of an anatomical structure, a direct mapping from the undeformed into the deformed state of the anatomical structure results.

3. MATERIAL PARAMETERS

By now, our implemented biomechanical model distinguishes two different materials, namely brain tissue and skull bone, which can be incorporated by assigning different values of the Lamé constants λ and μ to the corresponding subregions. In order to determine appropriate values for both materials, we carried out a comprehensive literature study, yielding the values summarized in Table 1. Most of the values given there were determined from other reported values,[21,23,24,26] mainly based on the works of Sauren and Classens[27] as well as Nagashima et al.[28] Other authors[16–20,25] incorporated real measured data, reported by, e.g., McElhaney et al.[29] or Nahum et al.[30] In our approach, where the deformations are driven by given correspondences, only the ratios of the values of λ and μ are necessary. In Table 2, the calculated ratios for the Lamé constant values given in Table 1 are summarized. Analyzing Table 2 reveals the interesting fact that only a small number of different Lamé constant ratios for brain tissue and skull bone exists. Application of these ratios in some initial synthetic experiments showed only slight differences in the resulting deformations. Thus, we concluded that the mean values of the ratios serve as valid estimates for the corresponding Lamé constants.

material parameter values	brain		skull	
article	$\lambda_{br}\,[kPa]$	$\mu_{br}\,[kPa]$	$\lambda_{sk}\,[kPa]$	$\mu_{sk}\,[kPa]$
Hosey and Liu 1982[16]	11101.8	22.2482	1334570	1842980
Ward 1982[17]	5270.27	219.595	1334570	1842980
Ruan et al. 1991[18]	540.811	22.5338	2093090	2663930
Willinger et al. 1992[19]	5472.97	228.041	1388890	2083330
Chu et al. 1994[20]	4110.74	83.8926	1805560	2708330
Tada et al. 1994[21]	8060.27	164.495	1466820	2025600
Takizawa et al. 1994[22]	41.7945	2.66773	-	-
Kuijpers et al. 1995[23]	8108.11	337.838	1805560	2708330
Kumaresan and Radhakrisnan 1996[24]	540.811	22.5338	1945000	2685950
Whitman et al. 1996[25]	-	-	180556	270833
Hartmann and Kruggel 1998[26]	12483.3	25.0167	2093090	2663930

Table 1. Reported values of the Lamé constants λ and μ for brain tissue and skull bone. Tada et al., Takizawa et al., as well as Hartmann and Kruggel distinguished originally between grey matter and white matter, but here, only the values for grey matter were given. A bar indicates that no values were given by the authors.

ratios of the material parameter values			
article	λ_{br}/μ_{br}	λ_{sk}/μ_{sk}	$\lambda_{sk}/\lambda_{br}$
Hosey and Liu 1982[16]	498.998	0.724137	120.212
Ward 1982[17]	24.0	0.724137	253.226
Ruan et al. 1991[18]	24.0	0.785715	3870.28
Willinger et al. 1992[19]	23.9999	0.666668	253.773
Chu et al. 1994[20]	49.0	0.666669	439.23
Tada et al. 1994[21]	49.0001	0.724141	181.981
Kuijpers et al. 1995[23]	24.0	0.666669	222.686
Kumaresan and Radhakrisnan 1996[24]	24.0	0.724139	3596.45
Hartmann and Kruggel 1998[26]	498.999	0.785715	167.671

Table 2. Calculated ratios for the Lamé constants for brain and skull tissue. Only those articles where material parameter values have been reported for both, brain tissue and skull bone, have been taken into consideration.

For the simulation of different anatomical structures, we have to determine appropriate ratios for the Lamé constants between those different structures. Following our previous practice for homogeneous materials, we calculated the ratios for the λ-values of skull bone and brain tissue and have also listed them in Table 2. Here, a larger variability the calculated ratios can be observed. However, it seems reasonable to choose again the mean value as ratio between the λ-values, while keeping the internal Lamé constant ratios of each material constant. To analyze the influence of our determined Lamé constant values on a deformation, we applied four parallel correspondences to a grid. These correspondences point in direction of the lower right corner of the grid and remain equal while different material properties were assumed. As indicated by the resulting grid deformations and calculated displacement vector fields in Figure 1, the material parameter values for homogeneous skull bone result in a significant stiffer behaviour compared to homogeneous brain tissue. By dividing the grid into two subregions Ω_1 and Ω_2, we get the result shown in Figure 1(c). In this case, the applied correspondences lead to a pure translation of the simulated bony rectangle, surrounded by soft brain material. The corresponding displacement vector field reveals, that the behaviour of the surrounding soft material is physically plausible: Along the path of translation, a stretching of the soft material occurs, while two vortices can be observed due to the lateral inflow of soft material.

4. EXPERIMENTS

Our approach has been tested on 2D synthetic images as well as real tomographic datasets. The synthetic experiments comprised different types of movements of a rigid object (e.g., translation, rotation, scaling, and shearing) embedded into an otherwise elastic material. Figure 2 depicts the deformation results for different types of translations. In

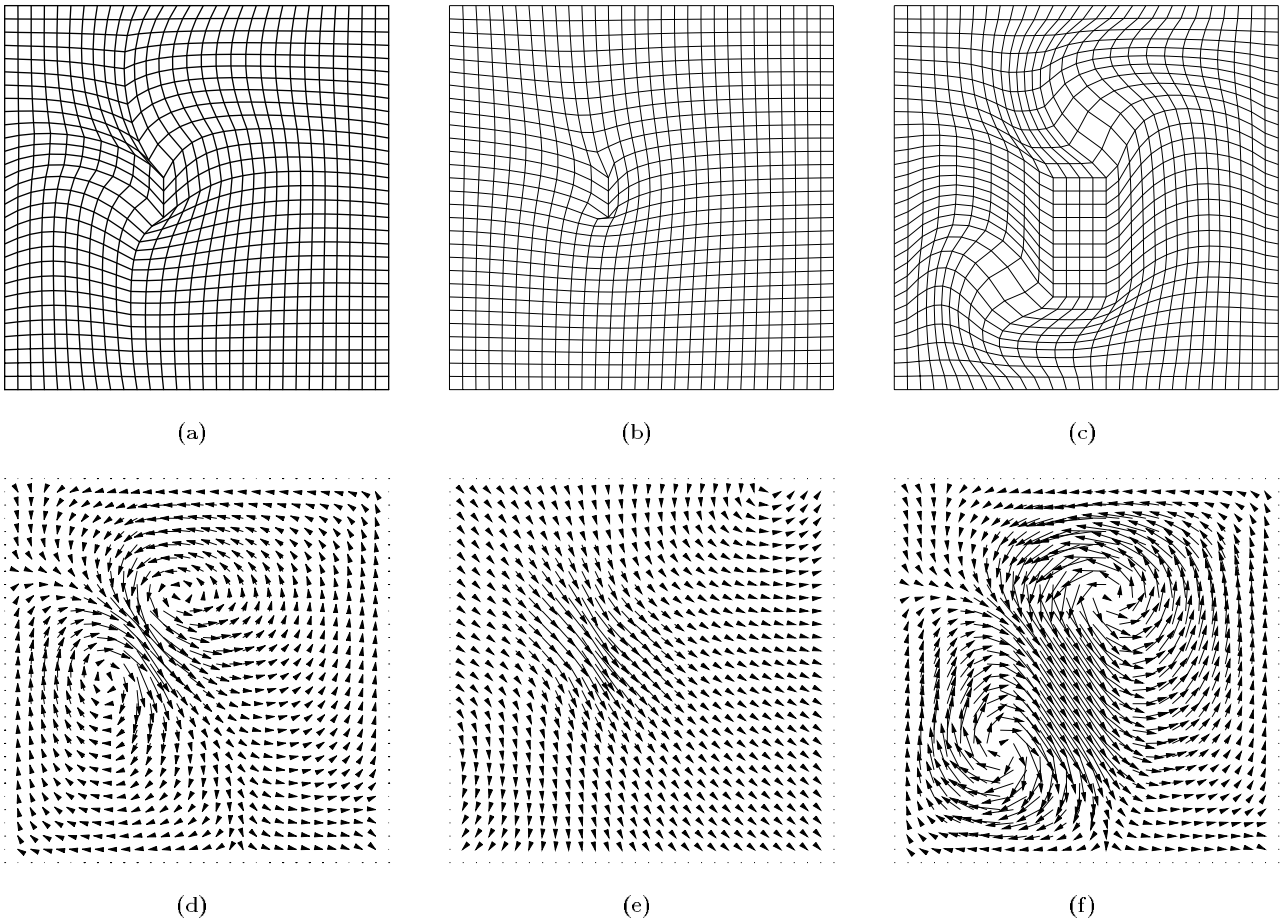

Figure 1. Resulting grid deformation (top row) and displacement vector field (bottom row) for four correspondences acting on the upper left part of the grid. Homogeneous Dirichlet boundary conditions were assumed at the grid boundaries. In (a) and (b) homogeneous areas of type brain tissue and skull bone were assumed, respectively. As expected, the assumed skull material results in a much stiffer behaviour. By spatially different Lamé constants, we can combine different materials as shown in (c). Here, a (simulated bony) rectangle embedded in simulated brain tissue results in a pure translation of the rectangle.

both cases, the star remains perfectly rigid while the surrounding soft material is deformed. Note that the visual impression of the broadening of the grid lines can be traced back to our resampling process. Some problems arise with objects rotated by an angle larger than 45°, see Figure 3. A possible explanation may be that the linear elasticity assumption of small deformations is violated in the experiments with large rotation angles.

For the experiments with real data, we used 2D pre- and postoperative MR images which were routinely acquired in conjunction with the planning and radiological control of a tumor resection. The postoperative image was used to simulate an intraoperative image. First, the corresponding tumor and resection area outlines were manually determined by a medical expert in both images, see Figures 4(a) and (b). Thereafter, a snake algorithm has been applied to determine the correspondences for these outlines, which then have been used as input for our model for the purpose of matching the pre- with the postoperative image. Figure 5(a) shows a locally erroneous registration result since only homogeneous soft material for the whole image was assumed. Especially in the vicinity of the ventricular system larger deviations are visible, see also the enlarged part of the ventricular system depicted in Figure 6(a).

In order to improve the registration result, different materials were incorporated by assigning spatially different Lamé constants λ and μ according to the underlying anatomical structures. To this end, the preoperative image was segmented with an interactive watershed algorithm[31] into four different regions, shown in Figure 4(c): combined

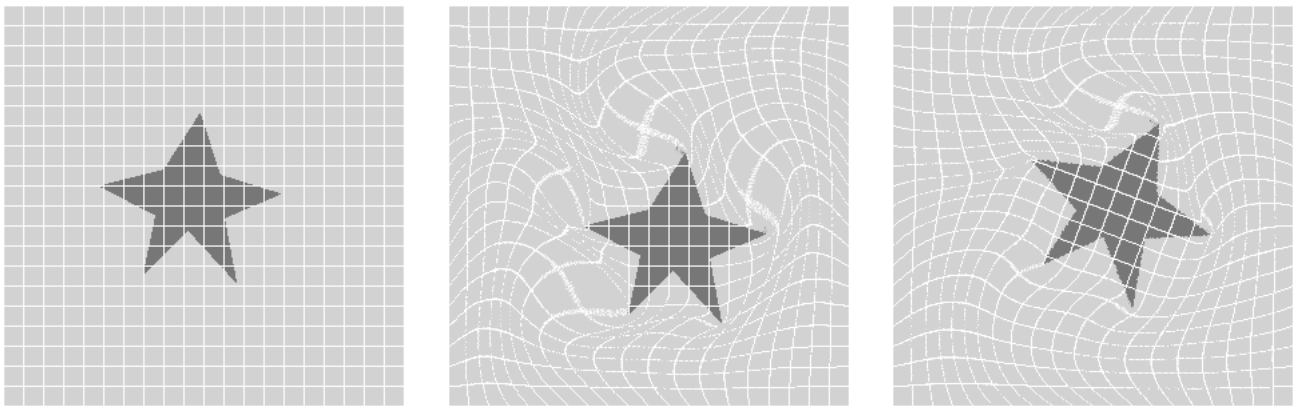

Figure 2. Predicted translation of a rigid star embedded into soft material (a) due to two given correspondences (b). In (c), only one correspondence was used, resulting in a translation and rotation of the star.

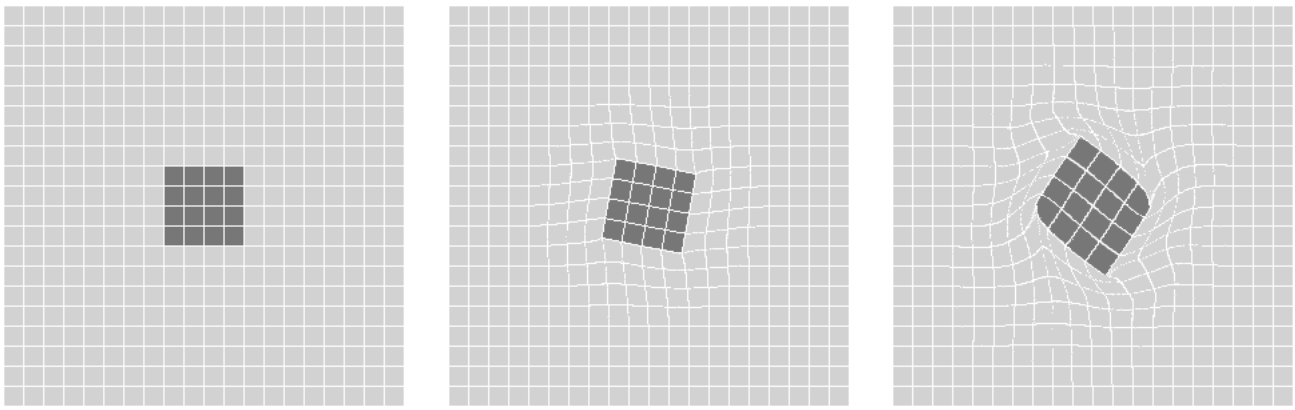

Figure 3. Predicted clockwise rotation of a rigid block embedded into soft material (a). The rotation angles were 10° and 45° in subfigures (b) and (c), respectively. In (c), the approach starts to fail as can be seen by the deformation of the overlaid grid lines inside the rigid block.

skin/skull region (white), brain (dark grey), CSF (light grey), and surrounding air, i.e. image background (black). For brain tissue and skull bone, the previously determined ratios were used, while CSF and air were roughly approximated as rigid and very soft materials, respectively. The result is shown in Figure 5(b) as well as 6(b). Here, a global movement of the head, forced by the given correspondences, can be observed which leads to a surprisingly poor registration result. However, this global movement can be suppressed by assuming a rigid image background, i.e. by assigning the Lamé constant values of a rigid body to the image background, see Figure 5(c). In this case, an overall good registration result can be achieved, even in the vicinity of the ventricular system, as can be seen clearly in Figure 6(c).

5. SUMMARY AND CONCLUSION

We proposed a novel biomechanical model of the human head based on linear elasticity theory to predict brain deformations due to surgical interventions. The model is driven by a set of given correspondences and incorporates

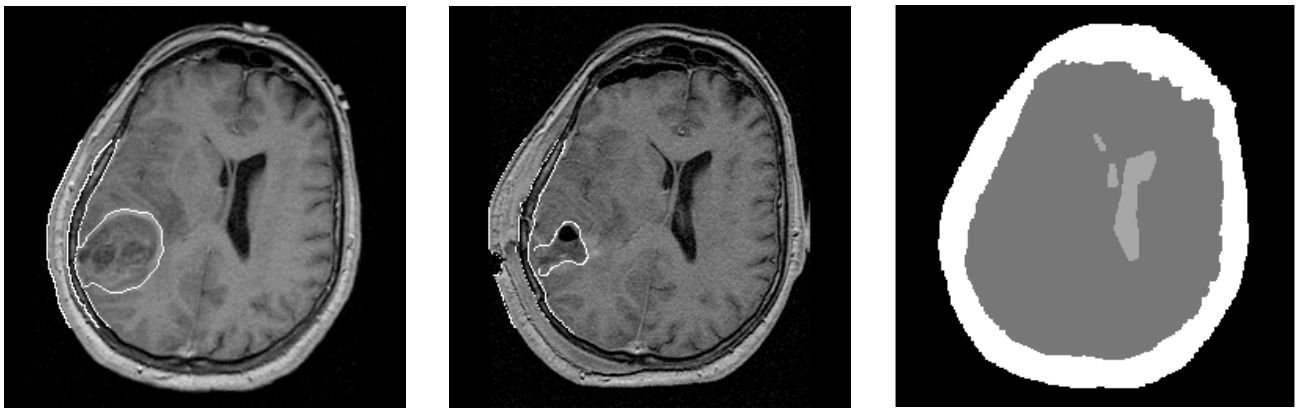

(a) (b) (c)

Figure 4. Manually determined outlines in the pre- (a) and postoperative (b) image. In (c), the segmented regions using an interactive watershed algorithm are depicted.

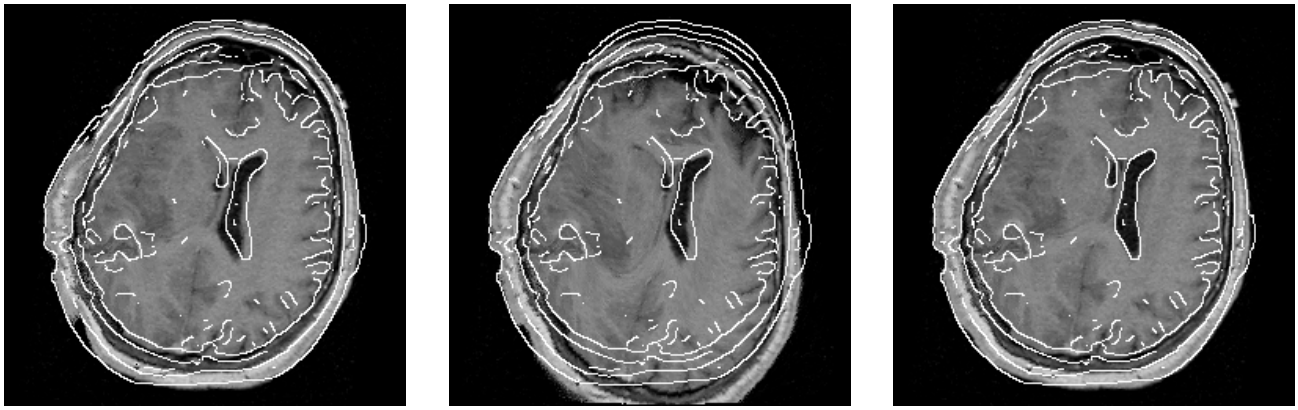

(a) (b) (c)

Figure 5. In (a), the registration result assuming homogeneous soft material properties (with overlaid Canny edges of the original postoperative image) is depicted. For the result shown in (b), inhomogeneous material properties based on the segmentation given in Figure 4(c) are assumed. The global head shift can be easily suppressed by assuming an artificial rigid image background, resulting in an overall good registration result in (c).

different material properties. Appropriate material parameter values were determined from the literature and experimentally validated. By carrying out experiments using synthetic as well as real medical images, it turns out that the approach leads to physically plausible deformation results. The incorporation of different anatomical structures leads to a significant enhancement of the registration result for the real MR images. We expect that the incorporation of more advanced constitutive equations leads to further improvements of the prediction results.

6. ACKNOWLEDGEMENT

Support of Philips Research Laboratories Hamburg, project IMAGINE (IMage- and Atlas-Guided Interventions in NEurosurgery), is gratefully acknowledged.

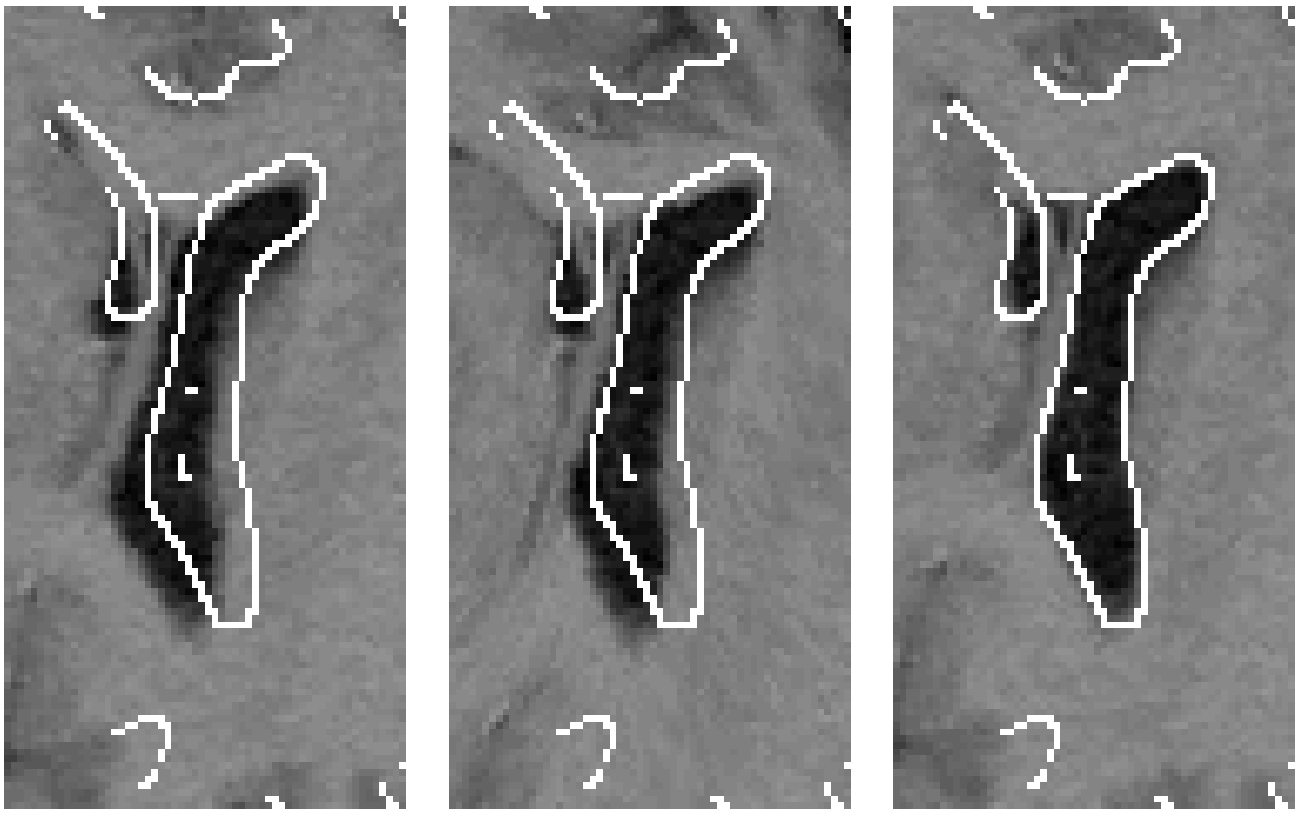

Figure 6. Enlarged parts of the ventricular systems of Figure 5 with overlaid Canny edges of the original postoperative image. Subfigure (a) shows the result for homogeneous soft material, (b) for the inhomogeneous case, and (c) for the inhomogeneous case with rigid image background. The improvement of the registration result is obvious.

REFERENCES

1. D. L. G. Hill, C. R. Maurer, R. J. Maciunas, J. A. Barwise, J. M. Fitzpatrick, and M. Y. Wang, "Measurement of Intraoperative Brain Surface Deformation under a Craniotomy," *Neurosurgery* **43**, pp. 514–526, September 1998.
2. R. D. Bucholz, D. D. Yeh, J. Trobaugh, L. L. McDurmont, C. Sturm, C. Baumann, J. M. Henderson, A. Levy, and P. Kessman, "The Correction of Stereotactic Inaccuracy Caused by Brain Shift Using an Intraoperative Ultrasound Device," in *Computer Vision, Virtual Reality and Robotics in Medicine and Medical Robotics and Computer-Assisted Surgery (CVRMed-MRCAS'97)*, J. Troccaz, E. Grimson, and R. Mösges, eds., vol. 1205 of *Lecture Notes in Computer Science*, pp. 459–466, Springer Verlag, (Grenoble, France), 1997.
3. P. J. Edwards, D. L. G. Hill, J. A. Little, and D. J. Hawkes, "Deformation for Image Guided Interventions Using a Three Component Tissue Model," in *Information Processing in Medical Imaging (IPMI'97)*, vol. 1230 of *Lecture Notes in Computer Science*, pp. 218–231, Springer Verlag, (Poultney, USA), March 1997.
4. C. Davatzikos, "Nonlinear Registration of Brain Images Using Deformable Models," in *Proceedings of the IEEE Workshop on Mathematical Methods in Biomedical Image Analysis (Cat. No. 96TB100056)*, pp. 94–103, (San Francisco, CA, USA), June 1996.
5. S. K. Kyriacou and C. Davatzikos, "A Biomechanical Model of Soft Tissue Deformation, with Applications to Non-rigid Registration of Brain Images with Tumor Pathology," in *Medical Image Computing and Computer-Assisted Intervention (MICCAI'98)*, W. M. Wells, A. Colchester, and S. Delp, eds., no. 1496 in Lecture Notes in Computer Science, pp. 531–538, Springer Verlag, October 1998.

6. M. Mooney, "A Theory of Large Elastic Deformation," *Journal of Applied Physics* **11**, pp. 582–592, September 1940.
7. K. K. Mendis, R. L. Stalnaker, and S. H. Advani, "A Constitutive Relationship for Large Deformation Finite Element Modeling of Brain Tissue," *Journal of Biomechanical Engineering* **117**, pp. 279–285, August 1995.
8. M. S. Estes and J. H. McElhaney, "Response of Brain Tissue to Compressive Loading," *American Society of Mechanical Engineers* **70-BHF-13**, pp. 1–4, 1970.
9. H. Lester, S. R. Arridge, and K. M. Jansons, "Local deformation metrics and nonlinear registration using a fluid model with variable viscosity," in *Proceedings of the Medical Image Understanding and Analysis (MIUA'98) Conference, Leeds, UK*, E. Berry, D. Hogg, K. V. Mardia, and M. A. Smith, eds., pp. 44–48, University of Leeds, July 1998.
10. O. Škrinjar, D. Spencer, and J. Duncan, "Brain Shift Modeling for Use in Neurosurgery," in *Medical Image Computing and Computer-Assisted Intervention (MICCAI'98)*, W. M. Wells, A. Colchester, and S. Delp, eds., no. 1496 in Lecture Notes in Computer Science, pp. 641–648, Springer Verlag, October 1998.
11. M. R. Pamidi and S. H. Advani, "Nonlinear Constitutive Relations for Human Brain Tissue," *Journal of Biomechanical Engineering* **100**, pp. 44–48, 1978.
12. Y. C. Fung, *Biomechanics: Mechanical Properties of Living Tissues*, Springer-Verlag, 1993.
13. C. Cuvelier, A. Segal, and A. A. van Steenhoven, *Finite Element Methods and Navier-Stokes Equations*, D. Reidel Publishing Company, 1986.
14. H. Kardestuncer and D. H. Norrie, *Finite Element Handbook*, McGraw-Hill Company, 1987.
15. W. Peckar, C. Schnörr, K. Rohr, and H. S. Stiehl, "Two-Step Parameter-Free Elastic Image Registration with Prescribed Point Displacements," *9th Int. Conf. on Image Analysis and Processing (ICIAP'97)* **1310**, pp. 527–534, 1997.
16. R. R. Hosey and Y. K. Liu, "A Homeomorphic Finite Element Model of the Human Head and Neck," in *Finite Elements in Biomechanics*, ch. 18, pp. 379–401, John Wiley & Sons, 1982.
17. C. C. Ward, "Finite Element Models of the Head and Their Use in Brain Injury Research," in *Proceedings of 26th Stapp Car Crash Conference*, pp. 71–85, (Ann Arbor, USA), 1982.
18. J. S. Ruan, T. B. Khalil, and A. I. King, "Human Head Dynamic Response to Side Impact by Finite Element Modeling," *Journal of Biomechanical Engineering* **113**, pp. 276–283, August 1991.
19. R. Willinger, C. M. Kopp, and D. Césari, "New concept of contrecoup lesion mechanism: modal analysis of a finite element model of the head," *Proceedings on Int. Res. Council Biokinetics Impacts* , pp. 283–298, September 1992.
20. C.-S. Chu, M.-S. Lin, H.-M. Huang, and M.-C. Lee, "Finite element analysis of cerebral contusion," *Journal of Biomechanics* **27**, pp. 187–194, February 1994.
21. Y. Tada, T. Nagashima, and M. Takada, "Biomechanics of brain tissue (simulation of cerebrospinal fluid flow)," *JSME International Journal, Series A (Mechanics and Material Engineering)* **37**, pp. 188–194, April 1994.
22. H. Takizawa, K. Sugiura, M. Baba, and J. D. Miller, "Analysis of Intracerebral Hematoma Shapes by Numerical Computer Simulation Using the Finite Element Method," *Neurologica Medico-Chirurgica* **34**, pp. 65–69, February 1994.
23. A. H. Kuijpers, M. H. A. Claessens, and A. A. H. J. Sauren, "The Influence of Different Boundary Conditions on the Response of the Head to Impact: A Two-Dimensional Finite Element Study," *Journal of Neurotrauma* **12**(4), pp. 715–724, 1995.
24. S. Kumaresan and S. Radhakrisnan, "Importance of partitioning membranes of the brain and the influence of the neck in head injury modelling," *Medical and Biological Engineering and Computing* **34**, pp. 27–34, January 1996.
25. T. A. Whitman, G. R. Wodicka, M. T. Morgan, and J. D. Bourland, "Measurement and Modeling of the Vibrational Response of the Ovine Head as it relates to Intracranial Pressure," in *Bridging Disciplines For Biomedicine*, 18th Annual International Conference of IEEE Engineering in Medicine and Biology Society, (Amsterdam, Netherlands), October 1996.
26. U. Hartmann and F. Kruggel, "Erste klinische Untersuchungen mit einem mechanischen Finite-Elemente-Modell des menschlichen Kopfes," in *Bildverarbeitung für die Medizin 1998*, T. Lehmann, V. Metzler, K. Spitzer, and T. Tolxdorff, eds., *Informatik aktuell*, pp. 59–63, Springer Verlag, March 1998.
27. A. A. H. J. Sauren and M. H. A. Claessens, "Finite element modeling of head impact: The second decade," in *Proceedings of the International IRCOBI, Conference on Biomechanics of Impact*, pp. 241–254, 1993.

28. T. Nagashima, T. Shirakuni, and S. I. Rapoport, "A Two-Dimensional Finite Element Analysis of Vasogenic Brain Edema," *Neurologica Medico-Chirurgica.* **30**, p. 1, 1990.
29. J. H. McElhaney, R. L. Stalnaker, and V. L. Roberts, "Biomechanical Aspects of Head Injury," *Human Impact Response* , pp. 85–112, 1973.
30. A. M. Nahum, R. Smith, and C. C. Ward, "Intracranial Pressure Dynamics During Head Impact," in *Proceedings of 21st Stapp Car Crash Conference*, pp. 339–366, 1977.
31. S. Tieck, S. Gerloff, and H. S. Stiehl, "Interactive graph-based editing of watershed-segmented 2D-images," in *1st Workshop on Interactive Segmentation of Medical Images (ISMI'98)*, 1998.